High resolution Thomson Parabola Spectrometer for full spectral capture of multi-species ion beams

Alejo, A., Kar, S., Tebartz, A., Ahmed, H., Astbury, S., Carroll, D. C., ... Borghesi, M. (2016). High resolution Thomson Parabola Spectrometer for full spectral capture of multi-species ion beams. Review of Scientific Instruments, 87(8), [083304]. DOI: 10.1063/1.4961028

Document Version:
Peer reviewed version

Queen's University Belfast - Research Portal:
Link to publication record in Queen's University Belfast Research Portal

High Resolution Thomson Parabola Spectrometer for Full Spectral Capture of Multi-Species Ion Beams

A. Alejo,[1] S. Kar,[1, a)] A. Tebartz,[2] H. Ahmed,[1] S. Astbury,[3] D.C. Carroll,[3] J. Ding,[2] D. Doria,[1] A. Higginson,[4] P. McKenna,[4] N. Neumann,[2] G.G. Scott,[3] F. Wagner,[5] M. Roth,[6] and M. Borghesi[1]

[1)] *Centre for Plasma Physics, School of Mathematics and Physics, Queen's University Belfast, BT7 1NN, UK*

[2)] *Institut für Kernphysik, Technische Universität Darmstadt, Schloßgartenstrasse 9, D-64289 Darmstadt, Germany*

[3)] *Central Laser Facility, Rutherford Appleton Laboratory, Didcot, Oxfordshire, OX11 0QX, UK*

[4)] *Department of Physics, SUPA, University of Strathclyde, Glasgow, G4 0NG, UK*

[5)] *GSI Helmholtzzentrum für Schwerionenforschung GmbH, Planckstraße 1, 64291 Darmstadt, Germany*

[6)] *Institut für Kernphysik, Technische Universität Darmstadt, Schloßgartenstraße 9, D-64289 Darmstadt, Germany*

(Dated: 27 July 2016)

We report on the experimental characterisation of laser-driven ion beams using a Thomson Parabola Spectrometer (TPS) equipped with trapezoidally-shaped electric plates, proposed by Gwynne *et al.* in Rev. Sci. Instrum. **85**, 033304 (2014). While a pair of extended (30 cm long) electric plates was able to produce a significant increase in the separation between neighbouring ion species at high energies, deploying a trapezoidal design circumvented the spectral clipping at the low energy end of the ion spectra. The shape of the electric plate was chosen carefully considering, for the given spectrometer configuration, the range of detectable ion energies and species. Analytical tracing of the ion parabolas matches closely with the experimental data, which suggests a minimal effect of fringe fields on the escaping ions close to the wedged edge of the electrode. The analytical formulae were derived considering the relativistic correction required for the high energy ions to be characterised using such spectrometer.

I. INTRODUCTION

Ion acceleration driven by high-power lasers has attracted a considerable interest over the last decade due to a range of potential applications in healthcare, industry, and science[1,2]. A number of ion acceleration mechanisms, such as Target Normal Sheath Acceleration (TNSA)[3–5], Radiation Pressure Acceleration (RPA)[6–8], Break-Out Afterburner (BOA)[9,10], and guided post-acceleration by laser-driven micro coils[11], are currently being subject of intense investigation, which are leading to significant progress towards the 100 MeV/n range[5]. These mechanisms inherently produce multi-species ion beams, due to the chemical composition of the target bulk and/or the contamination layer covering the target (typically containing hydrocarbons and water vapour)[12]. Among the ion diagnostics which are commonly used, such as radiochromic film stack[13], nuclear activation[14], or nuclear track detection[15,16], Thomson Parabola Spectrometer (TPS)[17] is arguably the most popular diagnostic due to their unique capability of spectrally characterising the ion beams while discriminating the species with different charge-to-mass ratio (Z/A).

As with any diagnostic, the resolution of a TPS is a key parameter in view of its use in a laser-driven ion acceleration experiment. In the case of TPSs, two types of resolution are of interest, viz. the energy resolution along a given trace (ion species), and the Z/A resolution - which defines the ability to discriminate two neighbouring ion traces. The Z/A resolution for a given TPS configuration varies across the range of energies resolved by the magnetic deflection, and becomes critical for high-energy ions (tens of MeV/nucleon)[18–20].

The separation between neighbouring ion traces can be increased by several ways, such as increasing the electric field strength or the length of the electric plates, or moving the detector farther away from the plates. However, as discussed in Gwynne *et al.*[19], increasing the length of the electric plates is the most effective route for increasing the Z/A resolution at high energies, while maintaining a compact design that can be fielded within the typical dimensions of an interaction chamber. Therefore, it was proposed in the ref. 19 to implement a pair of extended, trapezoidally-shaped electric plates, which will not only resolve ion traces at high energies, but will also retain the lower energy part of the spectrum by avoiding the spectral clipping typically associated to rectangular plates. The spectral clipping by the electrodes becomes progressively more significant as the length of the plates is extended. Although Gwynne *et al.*[19] demonstrated experimentally the effectiveness of extended electric plates, the effect of the trapezoidal electric plates was only explored by particle tracing simulations.

In this paper, we show the experimental characterisation of laser-driven multi-species ion beams employing a TPS with a pair of extended (30 cm-long) trapezoidal plates. The ion traces in the data closely match
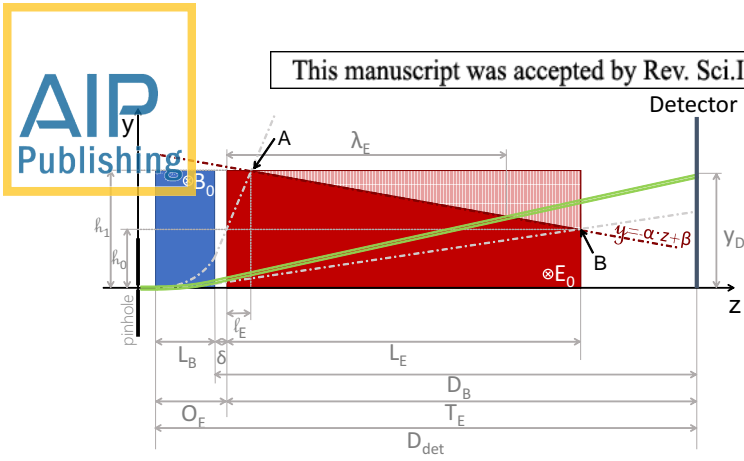
a)Electronic mail: s.kar@qub.ac.uk

FIG. 1. Schematic side view of a Thomson Parabola Spectrometer using trapezoidal electric plates.

with the analytical prediction, which suggest negligible fringe field effect despite the unconventional plate shape. Such extended-electrode ion spectrometers will be particularly useful for detecting high energy (hundreds of MeV/nucleon) multispecies ion beams, predicted from experiments employing multi-petawatt lasers in upcoming facilities[21,22]. For this reason, we implemented for the first time a fully relativistic treatment of the ion propagation within the TPS. The remaining of the paper is organised as follows. Sec. II describes the experimental setup and the design of the trapezoidally shaped electric plates considering the TPS dimensions and species of interest. The experimental results are discussed in Sec. III, and the relativistic analytical formula describing the shape of the ion traces on the detector is discussed in Sec. IV.

II. EXPERIMENTAL SETUP AND DESIGN OF THE TRAPEZOIDAL PLATES

The experiment was carried out at the Rutherford Appleton Laboratory (RAL), STFC, UK by employing the petawatt arm of the VULCAN laser system[23]. The data presented in this paper were obtained by irradiating the laser onto 25 μm thick aluminium foil targets. Using an $f/3$ off-axis parabolic mirror, the laser was focussed down to $\sim$ 6 μm full width at half maximum spots on the target, delivering a peak intensity in excess of 10^{20} W cm^{-2}. The TPS was placed at a distance of $\sim$106 cm along the target normal direction, along which direction the maximum ion energies are expected, TNSA being the main acceleration mechanism for the concerned target thickness and intensity here[24].

A schematic side view of a TPS with trapezoidal electric plates is shown in Fig. 1. A pinhole at the entrance of the diagnostic selects an ion pencil beam, which travels through regions of parallel magnetic (B_0) and electric (E_0) fields, both transverse to the beam axis. The magnetic field determines the position of the ions along the y-axis, depending on their energy per nucleon, while the electric field deflects the ions along the x-axis according to their charge-to-mass (Z/A) ratios. Considering that the electric and magnetic fields are homogeneous, the position of the ions reaching the detector can be analytically

derived (see Appendix V) as

$$x = \frac{\gamma}{\gamma^2 - 1} \frac{qE_0 L_E}{m_0 c^2} \left(T_E - L_E/2\right) , \qquad (1)$$

$$y = \frac{qB_0 L_B}{m_0 c\sqrt{\gamma^2 - 1}} \left(L_B/2 + D_B\right) , \qquad (2)$$

where q and m_0 are the charge and rest mass of the species of interest, γ is the Lorentz factor and L_B, D_B, T_E, and L_E are the dimensions of relevant sections of the TPS, as labelled in Fig. 1.

The line $y = -\alpha z + \beta$, where $\alpha = (h_1 - h_0)/(L_E - l_E)$ and $\beta = [h_1(L_E - O_E) - h_0(l_E + O_E)]/(L_E - l_E)$, defines the line along which rectangular electrodes were cut to make the trapezoidal shape. In order to find the optimum trapezoidal design for the electric plates, the locations at which different energy ions would impinge on the negatively-biased ($-V_b$) electrode were calculated for each of the relevant ion species. For a given separation between the beam axis and the negative electrode (Δ), the clipping position $(x, y, z) = \left(\Delta, y_e^{clip}, L_e^{clip}\right)$ can be expressed as

$$L_e^{clip} = \sqrt{\frac{\gamma^2 - 1}{\gamma} \frac{2\Delta\, m_0 c^2}{qE_0}} , \qquad (3)$$

$$y_e^{clip} = \frac{qB_0 L_B}{m_0 c\sqrt{\gamma^2 - 1}} \left(O_E - L_B/2 + L_e^{clip}\right) . \qquad (4)$$

In the experiment discussed here, we were interested in the characterisation of protons and carbon ions ($C^{\{4-6\}+}$), whose impinging position is plotted in Fig. 2(a). These curves were obtained for the TPS setup used in our experiment, i.e. using $B_0 \simeq 0.972$ T, $E_0 \simeq 20$ kV/cm, $L_B = 50$ mm, $O_E = 75$ mm, $L_E = 300$ mm, $\Delta \simeq 7$ mm, and $D_{det} = 493$ mm. For the usual rectangular plates (shown by the black dashed line in Fig. 2(a)), a significant range of ion energies would be blocked by the $-V_b$ electrode, which would produce partially clipped traces on the detector as shown in Fig. 2(b). Therefore, the modified design involves cutting off a section of the electrode, shown by the gray area in Fig. 2(a), so that the curves for all the species of interest lie above the electrode.

However, one has to be careful not to remove a larger section of the plate than necessary. The range of ion energies that one aims to unblock by creating a trapezoidal electrode shape depends on the given TPS setup. The minimum ion energy for a given species detectable by the detector depends on two factors, such as the finite size of the detector and the use of any filtering in front of the detector. Since Image Plate (IP) detectors were used in our case, which are sensitive to ambient lighting, the common practice is to wrap the IPs with a thin Al foil to avoid exposure to ambient light before the IP is scanned after the shot. The clipping position on the electrode for the lower energy cut-off for different ion species, due to either our detector size (70 mm×45 mm) or the stopping in the IP filter, are marked respectively as '◇' and '⋆' in Fig. 2(a). For each species, the minimum detectable energy would be the rightmost of the two points - whereas the detector size is the limiting factor for p$^+$ and C^{6+},
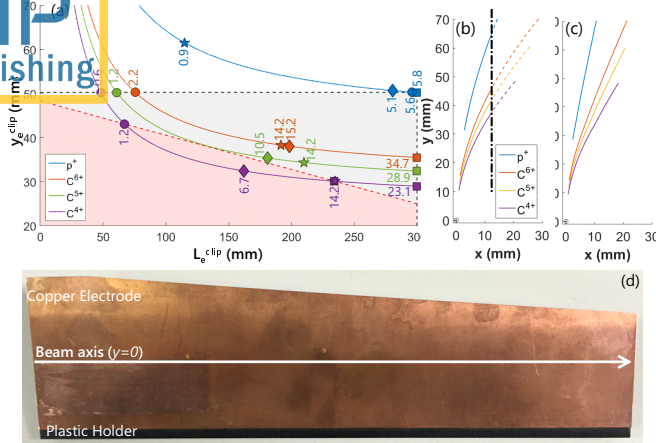
FIG. 2. **(a)** Graph plotting the positions on the plane of the $-V_b$ electrode (depth, L_e^{clip}, and height, y_e^{clip}) where ions would impinge depending on their Z, A and energy. The shape of the 30 cm-long rectangular electrode used in the experiment is shown by the black dashed line. The red dashed line represents the line along which the rectangular plate was cut to produce the trapezoidally shaped (red shaded area) electrode. The different markings on the curves represent the minimum (filled ○) and maximum (filled □) energies of ions clipped by the plates, the detection threshold due to the stopping in the IP filter (filled ⋆), and the finite detector size (filled ◇). The energy values in MeV are shown next to each marking. **(b)** and **(c)** show analytically plotted ion traces on the detector while using the 30 cm-long rectangular electrodes and the derived trapezoidal plates respectively. Dashed lines in (b) correspond to the region of the traces being clipped by the rectangular plates. **(d)** Picture of one of the trapezoidal electrodes used in the TPS during the experiment.

the filtering defines the cut-off energy for the C^{4+} and C^{5+} species.

With the aforementioned considerations, the final plate design was chosen, as shown by the red shaded area in Fig. 2(a), which would allow the entire detectable range of energies and species to reach the detector, producing unclipped traces as plotted in Fig. 2(c). The trapezoidal shaped electrodes thus used in the experiment were manufactured from a 1 mm-thick copper sheet, mounted on a plastic holder as shown in Fig. 2(c).

In the experiment, the TPS was fielded with BAS-TR imaging plates as detectors, which were wrapped with 12 μm-thick Al foil to avoid accidental exposure to ambient light after the irradiation. The IPs were scanned 60-90 minutes after the irradiation, using a commercial IP scanner (Fujifilm FLA-5000[25]), with a 16-bit dynamic range and a 25 μm × 25 μm pixel size. The measured signal was converted from the scan value (or quantum level (QL)) to PSL using the formula given by the manufacturer[20,26], and then was corrected for the fading of the signal due to spontaneous decay[20,27].

III.   EXPERIMENTAL RESULTS

In the experiment, three electrode designs were tested to compare the results obtained with each of them on a

proof-of-principle basis. Initially, a TPS with 150 mm-long rectangular electric plates was used to characterise the laser-driven ion beams, the data from which is shown in Fig. 3(a).

Although the C^{6+} and C^{4+} traces in this shot were well separated, this set-up would have been ineffective in discriminating these traces at the higher energies expected from optimized targets, advanced mechanisms and/or at higher power laser facilities. The maximum C^{6+} energy that can be distinguished from the neighbouring traces in the current TPS would have been 198 MeV (16.5 MeV/nucleon). It is to be noted that, due to the limitations in laser performance encountered during this campaign, the maximum proton and carbon energies obtained from this shot were 28 MeV and 102 MeV respectively, which are significantly less than what can be obtained from the TNSA mechanism[4], or from ultra-thin (sub-micron) targets at such laser systems[7].

The electrodes were exchanged for 300 mm-long rectangular electric plates in the following step (Fig. 3(b)), keeping the same O_E distance. It can be clearly seen by comparing the data shown in Fig. 3(a) and 3(b), how the separation between the different traces at the high-energies was enlarged. The improvement in the trace separation, and the possibility of discriminating traces at high energies (around 100 MeV/nucleon) can be seen from the simulated traces, which match well with the experimental data for lower energies. The only issue with such setup is, however, the clipping of the lower energy part of the ion traces by the extended electrodes, which appears as a sharp vertical cut-off of the data as shown in Fig. 3(b). A precise measurement of the distance between the ion-beam axis and the $-V_b$ electrode (Δ) can be obtained from the clipping position, $\Delta = 6.7 \pm 0.5$ mm, which agrees with the measurement taken during the setup.

Finally, the electrodes were replaced by the trapezoidal plates, made according to the optimised design discussed in Sec. II. The experimental result obtained using these trapezoidal electrodes is shown in Fig. 3(c). As expected, the separation between the traces in this case matches exactly with that obtained with the rectangular long plates, but without the clipping of lower energy part of the traces. Where the finite size of the detector limits the minimum detectable energy for species such as p^+ or C^{6+}, the C^{4+} trace faded within the detector field of view due to the stopping of the low energy ions inside the IP filter. One can also find the presence of faint traces of C^{5+} and O^{6+}, as shown in the zoomed-in view in Fig. 3(d), which were well separated. Unfortunately the ion energy in this shot was too low, again due to shot-to-shot variation in laser performance during the campaign, to show a set of well-separated, unclipped traces extending to higher energies. However, the data clearly shows the expected advantage arising from the use of trapezoidal electrodes.
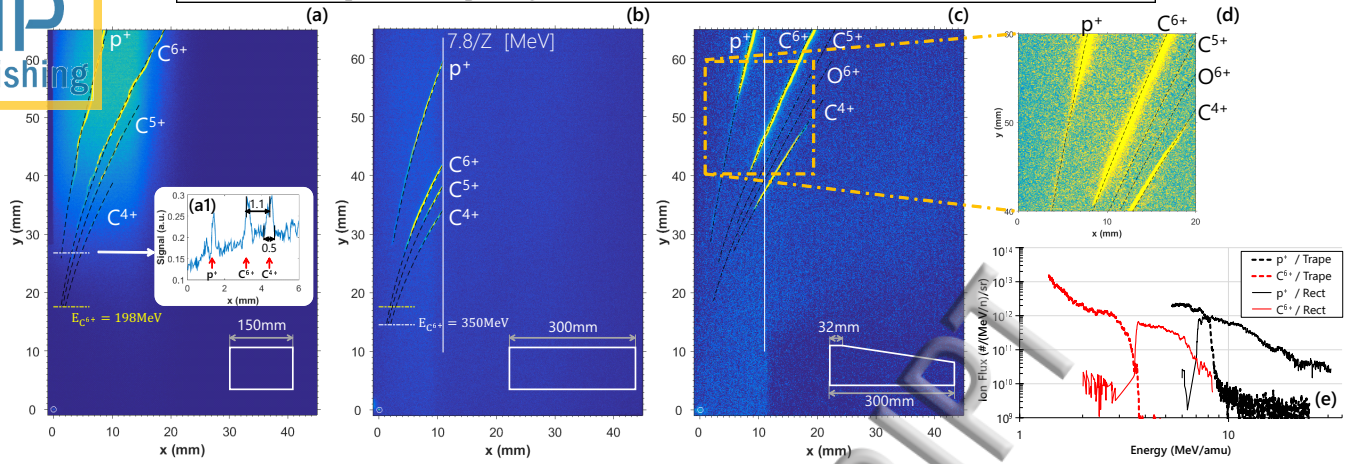
FIG. 3. (**a-c**) Experimental raw data from the IP scans using different designs of the electric plates, as drawn in the bottom right corner of each image. Black dashed lines show the fit to the ion traces using the analytical formulae mentioned in the text. (**a1**) shows a line-out across the ion traces along the white dashed line in (a). The white vertical line in (b) shows the position of the sharp cut-off in the ion traces shadowed by the electrode. (**d**) Zoomed-in view of a part of the data shown in (c), as marked by the orange dashed square. (**e**) Spectra of proton (black) and carbon (red) ions retrieved from the TPS using the rectangular (solid line) and trapezoidal (dashed) electric plates.

IV. COMPARISON BETWEEN EXPERIMENTAL AND ANALYTICAL TRACES

While employing trapezoidal electric plates, the part of the trace formed by the ions passing over the electrode does not follow the same parabolic curve defined by the higher energy part of the trace. This is due to the lower energy ions effectively experiencing the electric field region over a different propagation length than the higher energy ions. Therefore, such design would not be useful without an analytical method to retrieve the ion spectra. Assuming λ_E to be the length of the electric field region experienced by a given ion, the position of the ion on the detector can be written as (by substituting λ_E in place of L_E in Eq. 1).

$$x = \frac{\gamma}{\gamma^2 - 1} \frac{qE_0\lambda_E}{m_0 c^2} (T_E - \lambda_E/2) . \quad (5)$$

The variable λ_E is given by the z-position at which the particle exits the electric-field region, and therefore can be expressed as

$$\lambda_E = \begin{cases} \frac{\beta + L_B \cdot \Phi}{\alpha + 2\Phi} - O_E & , \ E_{lim}^A \leq E \leq E_{lim}^B \\ L_E & , \ E \geq E_{lim}^B \end{cases} , \quad (6)$$

where α and β define the line along which the electrodes were cut (Fig. 1), and the dimensionless factor Φ is given by $\Phi = qB_0L_B/\left(2m_0c\sqrt{\gamma^2-1}\right)$. The limits E_{lim}^A and E_{lim}^B define the energy range for which the ions exit the electric field region through the chopped side of the plate, corresponding to the points A and B in Fig. 1, respectively. For energies higher than E_{lim}^B, the particles will leave the plates through the longest region, experiencing a constant plate length of L_E independent of their energy. On the other end, for energies below E_{lim}^A, the Larmor radius will cause the particles to leave the electric field through the top flat section of the plates. The values for

both energy limits can be derived as shown in Eq. 7.

$$\frac{E_{lim}^A}{m_0 c^2} = \sqrt{\left[\frac{qB_0L_B\left[O_E + l_E - L_B/2\right]}{m_0 c h_1}\right]^2 + 1} - 1 ,$$

$$\frac{E_{lim}^B}{m_0 c^2} = \sqrt{\left[\frac{qB_0L_B\left[O_E + L_E - L_B/2\right]}{m_0 c h_0}\right]^2 + 1} - 1 . \quad (7)$$

The ion traces on the detector for the TPS with trapezoidally-shaped electrodes can then be defined by using the formulae in Eqs. 5 and 2. These formulae are based on the approximation of a homogeneous electric field inside the region between the two trapezoidal electrodes and zero electric field elsewhere, i.e. ignoring the fringe fields appearing close to the wedged-side of the electrodes. However, the ion traces derived using Eqs. 5 and 2, depicted by the dashed lines in Fig. 3(c) and (d), show a good agreement with the experimental traces. Therefore, it is reasonable to ignore any fringe effects around the plates for the range of energies of concern.

Although the ion traces produced by the TPS with trapezoidal electrodes do not follow a parabolic trajectory in the lower energy range, one can identify the ion species corresponding to a given trace by either considering the parabolic part of the trace, or by using the modified TPS formulae given by Eqs. 5 and 2. Once the ion trace is identified and isolated from the rest of the data, one can obtain the ion spectrum on the basis of the magnetic field deflection and the detector calibration. As an example, the p^+ and C^{6+} spectra obtained from the data shown in Figs. 3(b) and 3(c) are shown in Fig. 3(e). As it can be seen here, using trapezoidal shaped electrode allowed detecting the lower energy part of the ion spectrum, which would be otherwise clipped when using a rectangular shaped electrode. The capability of detecting lower energy ions may also be valuable as a monitoring tool for failed or low efficiency shots, where obtaining some spectral information may aid understanding the causes for the low performance in accelerating ions.

CONCLUSIONS

The ongoing advances in laser-driven ion acceleration, coupled with the prospect of significant progress at upcoming laser facilities are leading to the need for a compact ion spectrometers for characterisation of multi-species, high energy ion sources, capable of resolving ion species at high energies ($10s - 100$ MeV/nucleon). Here we have presented the experimental demonstration of a modified TPS design with trapezoidally-shaped electrodes, proposed by Gwynne *et al.*[19]. The method for designing an optimised electrode shape for our experimental setup is discussed, along with an analytical formulation for simulating the ion traces produced by such TPS. The analytically plotted ion traces match closely with the experimental data, proving that minimal fringe-field effects on the ions escaping over the wedged side of the trapezoidal electrodes are not significant. The proposed analytical treatment takes consideration of the relativistic corrections required for very high energy ($\gtrsim 100$ MeV/nucleon) ions, expected in the near future from interactions involving multi-petawatt lasers at upcoming facilities.

ACKNOWLEDGEMENTS

V. ANALYTICAL DERIVATION OF THE TPS EQUATIONS

The trajectory of ions passing through a TPS is solved using Newton's laws. In order to obtain the parabolic shape of the ion traces observed on the detector[19,20], a low magnetic field approximation is commonly used, in which the Larmor radius (R_L) is large enough ($\gg L_B$) to consider $v_y \ll v_z$.

In case of a relativistic particle of rest mass m_0, charge q and kinetic energy U entering a TPS, the acceleration experienced by the particle can be written as

$$\vec{a} = \frac{1}{m_0 \gamma(\vec{v})} \left[\vec{F} - \left(\vec{\beta} \cdot \vec{F} \right) \vec{\beta} \right], \qquad (8)$$

where γ is the Lorentz factor and $\vec{F} = q \left(\vec{E} + \vec{v} \times \vec{B} \right)$ is the Lorenz force experienced by the particle inside the homogeneous electric and magnetic fields.

Since the energy gain from the electric field is negligible ($\Delta U \leq ZeV_0 \ll m_0 c^2$), $\vec{\beta}$ and $\gamma = 1 + U/m_0 c^2$ can be assumed to be constant during its transit inside the TPS diagnostic. The term $\vec{\beta} \cdot \vec{F}$ in Eq. 8 for different regions

inside the TPS can be expressed as

$$\vec{\beta} \cdot \vec{F} \sim \begin{cases} \vec{\beta} \cdot \vec{E} = \beta_x E_0 \ll E_0 & \vec{E} = E_0 \hat{x}, \vec{B} = 0 \\ \vec{\beta} \cdot \left(\vec{\beta} \times \vec{B} \right) = 0 & \vec{E} = 0, \vec{B} = B_0 \hat{x} \\ 0 & \vec{B} = \vec{E} = 0 \end{cases} \quad (9)$$

Therefore, for a relativistic particle diagnosed by a TPS, the acceleration can simply be expressed as Newton's law with a correction for the *inertial mass*,

$$\vec{a} = \frac{1}{m_0 \gamma} \vec{F}. \qquad (10)$$

The low magnetic field approximation mentioned above also upholds for the relativistic particles, as the condition, $R_L = m_0 c \sqrt{\gamma^2 - 1}/qB_0 \gg L_b$, remains valid for the typical parameters (few Tesla magnetic field strength extended over tens of centimetres) used in experiments.

Under these considerations, the equations of motion along different axes can be written analytically as

$$x = \frac{qE_0 L_E}{\gamma m_0 v_z^2} \left(T_E - L_E/2 \right) \qquad (11)$$

$$y = \frac{qB_0 L_B}{\gamma m_0 v_z} \left(L_B/2 + D_B \right), \qquad (12)$$

Using $\gamma v_z = c\sqrt{\gamma^2 - 1}$ and $\gamma v_z^2 = c^2 \cdot (\gamma^2 - 1)/\gamma$, one can rewrite the equations as shown in Eqs. 1, 2.

[1] A. Macchi, M. Borghesi, and M. Passoni, Reviews of Modern Physics **85**, 751 (2013).

[2] H. Daido, M. Nishiuchi, and A. S. Pirozhkov, Report on Progress in Physics **75**, 056401 (2012).

[3] J. Fuchs, P. Antici, E. dHumières, E. Lefebvre, M. Borghesi, E. Brambrink, C. Cecchetti, M. Kaluza, V. Malka, M. Manclossi, *et al.*, Nature Physics **2**, 48 (2005).

[4] L. Robson, P. Simpson, R. Clarke, K. Ledingham, F. Lindau, O. Lundh, T. McCanny, P. Mora, D. Neely, C.-G. Wahlström, *et al.*, Nature Physics **3**, 58 (2006).

[5] F. Wagner, D. O, Brabetz, P. Fiala, A. Kleinschmidt, P. Poth, V. Schanz, A. Tebartz, B. Zielbauer, M. Roth, T. Sthlker, and V. Bagnoud, Physical Review Letters **116**, 205002 (2016).

[6] A. Robinson, M. Zepf, S. Kar, R. Evans, and C. Bellei, New Journal of Physics **10**, 013021 (2008).

[7] S. Kar, K. Kakolee, B. Qiao, A. Macchi, M. Cerchez, D. Doria, M. Geissler, P. McKenna, D. Neely, J. Osterholz, *et al.*, Physical Review Letters **109**, 185006 (2012).

[8] J. Bin, W. Ma, H. Wang, M. Streeter, C. Kreuzer, D. Kiefer, M. Yeung, S. Cousens, P. Foster, B. Dromey, *et al.*, Physical Review Letters **115**, 064801 (2015).

[9] L. Yin, B. Albright, B. Hegelich, and J. Fernández, Laser and Particle Beams **24**, 291 (2006).

[10] L. Yin, B. Albright, K. Bowers, D. Jung, J. Fernández, and B. Hegelich, Physical Review Letters **107**, 045003 (2011).

[11] S. Kar, H. Ahmed, R. Prasad, M. Cerchez, S. Brauckmann, B. Aurand, G. Cantono, P. Hadjisolomou, C. L. Lewis, A. Macchi, *et al.*, Nature Communications **7**, 10792 (2016).

[12] S. Gitomer, R. Jones, F. Begay, A. Ehler, J. Kephart, and R. Kristal, Physics of Fluids **29**, 2679 (1986).

[13] F. Nürnberg, M. Schollmeier, E. Brambrink, A. Blažević, D. Carroll, K. Flippo, D. Gautier, M. Geissel, M. Harres, B. Hegelich, *et al.*, Review of scientific instruments **80**, 033301 (2009).

[14] R. Clarke, P. Simpson, S. Kar, J. Green, C. Bellei, D. Carroll, B. Dromey, S. Kneip, K. Markey, P. McKenna, *et al.*, Nuclear Instruments and Methods in Physics Research Section A: Accelerators, Spectrometers, Detectors and Associated Equipment **585**, 117 (2008).

[15]R. Fleischer, P. Price, and R. Walker, Journal of applied Physics **36**, 3645 (1965).

[16]L. Kar, M. Borghesi, L. Romagnani, S. Takahashi, A. Zayats, V. Malka, S. Fritzler, and A. Schiavi, Journal of applied physics **101**, 044510 (2007).

[17]J. J. Thomson, Proceedings of the Royal Society of London. Series A **89**, 1 (1913).

[18]D. Carroll, P. Brummitt, D. Neely, F. Lindau, O. Lundh, C.-G. Wahlström, and P. McKenna, Nuclear Instruments and Methods in Physics Research Section A: Accelerators, Spectrometers, Detectors and Associated Equipment **620**, 23 (2010).

[19]D. Gwynne, S. Kar, D. Doria, H. Ahmed, M. Cerchez, J. Fernandez, R. Gray, J. Green, F. Hanton, D. MacLellan, P. McKenna, Z. Najmudin, D. Neely, J. Ruiz, A. Schiavi, M. Streeter, M. Swantusch, O. Willi, M. Zepf, and M. Borghesi, Review of Scientific Instruments **85**, 033304 (2014).

[20]A. Alejo, S. Kar, H. Ahmed, A. Krygier, D. Doria, R. Clarke, J. Fernandez, R. Freeman, J. Fuchs, A. Green, J. Green, D. Jung, A. Kleinschmidt, C. Lewis, J. Morrison, Z. Najmudin, H. Nakamura, G. Nersisyan, P. Norreys, M. Notley, M. Oliver, M. Roth, J. Ruiz, L. Vassura, M. Zepf, and M. Borghesi, Review of Scientific Instruments **85**, 093303 (2014).

[21]D. Papadopoulos, C. Le Blanc, G. Chériaux, P. Georges, G. Menerat, J. P. Zou, F. Mathieu, and P. Audebert, in *Advanced Solid State Lasers* (Optical Society of America, 2013) pp. ATu3A–43.

[22]"Extreme light infraestracture(eli)," http://www.eli-np.ro//.

[23]C. Danson, P. Brummitt, R. Clarke, J. Collier, B. Fell, A. Frackiewicz, S. Hancock, S. Hawkes, C. Hernandez-Gomez, P. Holligan, M. Hutchinson, A. Kidd, W. Lester, I. Musgrave, D. Neely, D. Neville, P. Norreys, D. Pepler, C. Reason, W. Shaikh, T. Winstone, R. Wyatt, and B. Wyborn, Nuclear Fusion **44**, S239 (2004).

[24]S. Wilks, A. Langdon, T. Cowan, M. Roth, M. Singh, S. Hatchett, M. Key, D. Pennington, A. MacKinnon, and R. Snavely, Physics of Plasmas **8**, 542 (2001).

[25]"Fujifilm bas-tr imaging plates," http://www.fujifilm.com ().

[26]"Information about conversion of ip scanner readout to psl," http://beamline.harima.riken.jp/bl45xu/web_old/Info/BAS2500imgSpec.pdf ().

[27]D. Doria, S. Kar, H. Ahmed, A. Alejo, J. Fernandez, M. Cerchez, R. J. Gray, F. Hanton, D. A. MacLellan, P. McKenna, Z. Najmudin, D. Neely, L. Romagnani, J. A. Ruiz, G. Sarri, C. Scullion, M. Streeter, M. Swantusch, O. Willi, M. Zepf, and M. Borghesi, Review of Scientific Instruments **86**, 123302 (2015).

(a)

p^+

C^{6+}

C^{5+}

C^{4+}

(a1)

1.1

0.5

Signal (a.u)

p^+ C^{6+} C^{4+}

x (mm)

$E_{C6+} = 198 MeV$

150mm

y (mm)

x (mm)

(b)

7.8/Z [MeV]

p^+

C^{6+}
C^{5+}
C^{4+}

$E_{C6+} = 350 MeV$

300mm

y (mm)

x (mm)

(c)

p^+ C^{6+} C^{5+}

O^{6+}

C^{4+}

32mm

300mm

y (mm)

x (mm)

(d)

p^+ C^{6+}

C^{5+}

O^{6+}

C^{4+}

y (mm)

x (mm)

(e)

Ion Flux (#/(MeV/n)/sr)

- - - p^+ / Trape
- - - C^{6+} / Trape
—— p^+ / Rect
—— C^{6+} / Rect

Energy (MeV/amu)

(a)

(b)

(c)

(d)

Copper Electrode

Beam axis (y=0)

Plastic Holder